J Mater Sci: Mater Med (2008) 19:2223–2229
DOI 10.1007/s10856-007-3279-z

Fabrication of biphasic calcium phosphates/polycaprolactone composites by melt infiltration process

Byong-Taek Lee · Do Van Quang · Min-Ho Youn · Ho-Yeon Song

Received: 8 February 2007 / Accepted: 18 September 2007 / Published online: 1 December 2007

Abstract Synthesis and characterization of material properties of biphasic calcium phosphates (BCP)/polycaprolactone (PCL) composites, which were obtained by melt infiltration of PCL using porous BCP bodies, were investigated. Using 70 vol.% of poly methyl methacrylate (PMMA) powder as a pore-forming agent, porous BCP bodies were obtained by pressure less sintering depending on the temperature. The porous bodies obtained showed interconnected, spherical pores about 200 μm in diameter. Densification of the pore frame improved and grain growth increased remarkably as the sintering temperature increased. Molten PCL was infiltrated into porous BCP bodies to obtain the BCP/PCL composites. The material properties such as the relative density, hardness, bending strength, and elastic modulus of BCP/PCL composite, which was sintered at 1200 °C, were 95.7%, 11.2 Hv, 31.6 MPa and 10.2 GPa, respectively.

1 Introduction

Biphasic calcium phosphates (BCP) have been widely used as artificial bone and bone substrates because their chemical compositions are similar to human bone. BCP bioceramic, composed of β-tricalcium phosphate (β-$Ca_3(PO_4)_2$, β-TCP) and hydroxyapatite ($Ca_{10}(PO_4)_6(OH)_2$, HAp), has some desirable properties, such as excellent biocompatibility, bioactivity, and osteoconduction [1–6]. In addition, polycaprolactone (PCL) is a typical biodegradable polymer with excellent biocompatibility [7, 8]. Due to its orderly and compliant chains, PCL shows relatively strong crystallization and low melting temperature. Thus, it is very hydrophobic and degrades at a slower rate than either polylactic or polyglycolic acid [9]. Hence, PCL has been widely used for bone substitutes and drug carriers.

In the human body, the crystallinity, porosity, and composition of bone are parameters, which influence the mechanical properties of human bone. The mechanical properties of synthetic calcium phosphates are decided by their crystallinity, porosity, composition, and grain size as well. The mechanical properties of synthetic calcium phosphates decrease significantly with decreasing crystallinity, high porosity, and coarse grain size [9]. Specifically, high crystallinity, low porosity, and small grain size tend to result in more stiffness, but greater compressive and tensile strengths.

Recently, there are many reports showed that there was no inflammation around the implanted BCP surrounded with bone tissues [10, 11]. This result indicated that BCP plays the roles of support and filler of bone and can become a part of the bone skeleton. Thus, the infiltration of PCL into the porous BCP body can improve the fracture strength as well as the brittleness of porous BCP bodies, which are main factors for clinical applications [9, 12–15]. Furthermore, the combination of BCP and PCL is being considered as a promising approach to fabricate excellent biomedical materials for application in load-bearing parts [13].

B.-T. Lee (✉) · D. Van Quang · M.-H. Youn
Department of Biomedical Engineering and Materials, School of Medicine, Soonchunhyang University, 366-1, Ssangyoung-dong, Cheonan, Chungnam 330-090, South Korea
e-mail: lbt@kongju.ac.kr

H.-Y. Song
Department of Microbiology, School of Medicine, Soonchunhyang University, 366-1, Ssangyoung-dong, Cheonan, Chungnam 330-090, South Korea

In this work, BCP/PCL composites were fabricated by melt infiltration process to improve the material properties of porous BCP bodies which was produced using spherical-shaped polymethyl methacrylate (PMMA) powder as a pore-forming agent. The present work is focused on the characterization of the relationship between the microstructure and material properties by measuring their elastic modulus and bending strength.

2 Experimental procedure

To obtain porous BCP composites, spherical BCP powder (about 80 nm) synthesized by a microwave-assisted process [15] and PMMA (range about 150–250 μm, LG chemical company, Korea) as a pore-forming agent were used. First, BCP powder and polyethylene glycol 400 liquid (PEG—5 wt.% of BCP powder, Junsei chemical Co.,Ltd, Japan) [16], which was used to increase strength of green pellets, were mixed for 24 h by wet ball-milling using Al_2O_3 ball, and then the mixture powders were dried on a hot plate while stirring. Next, the mixture powders of BCP and PEG and 70 vol.% of PMMA powder were mixed for 15 h by dry ball-milling also using Al_2O_3 balls. They were compacted into pellets by a uni-axial press. The green pellets were burned out in air atmosphere at 700 °C and the heating rate was 30 °C/h. Finally, the burn-out samples were sintered at different temperatures (1,200 and 1,400 °C) in air atmosphere.

On the other hand, PCL (Aldrich, USA) was melted at 120 °C, and then the melted PCL was poured into a mold, which contained porous BCP. The temperature was kept the same as the melt temperature of PCL for about 5–10 min before natural cooling. After complete solidification of melted PCL, the PCL on the outside of the samples was removed to take the BCP/PCL composites.

For the analysis of the PMMA and PCL weight loss depending on the increase of temperature, thermo-gravimetric and differential thermal analysis (TG/ DTA, SDT Q600, TA instruments) were used with 10 °C/min of heating rate in air atmosphere. The relative densities of the porous BCP bodies were measured by the Archimedes method, but that of the BCP/PCL body was measured by the mass and dimensions. The pore size and microstructure of the porous BCP and BCP/PCL composites were investigated by scanning electron microscopy (SEM, JSM-635F, Jeol) on the polished surface of the sample which was polished using sand paper (raw polishing) and diamond polishing wheel (3 and 1 μm). To identify the crystal structure and phases, an X-ray diffractometer (XRD, D/MAX-250, Rigaku, Japan) were used with CuKα radiation at 40 kV and 100 mA. The hardness was measured using a Vickers hardness tester (Hv-112, Akashi, Japan) by indentation with a load of 0.3 kg (10 points/sample). For bending strength and elastic modulus measurements, the samples were made with a bar shape ($4 \times 4 \times 35$ mm^3). The bending strength measurement was carried out using a four-point bending method with a span length of 10 mm and a crosshead speed of 0.1 mm/min, using a universal testing machine (Unitech^{TM}, R&B, Korea). The elastic modulus was calculated using the following equation, which was developed by Grindosonic (J. W. Lemmens, MKS) [17].

$$E_R = 0.9465 \times \frac{M \times f^2}{w} \times \frac{L_T^3}{t^3} \times [1 + 6.59 \times (\frac{t^2}{L_T^2})]$$

where E_R is the elastic modulus, M is the weight, f is the frequency, w is the width, L_T is the length and t is the thickness of the specimen. When the elastic modulus was calculated, average values (more than 10 times) were used.

3 Results and discussion

Figure 1 shows SEM micrographs of (a) raw BCP and (b) raw PMMA powders. The particle sizes of raw BCP powder were about 70–90 nm in diameter, respectively. On the other hand, the PMMA powder, which was used as a pore-forming agent, was spherical-shaped and about 150–250 μm in diameter.

Figure 2 shows TG/DTA profiles of (a) PCL, (b) PMMA powders, and (c) green pellet. In Fig. 2a, the TG profile shows that the percentage of weight of PCL decreased as the temperature increased to 250 °C, and when the temperature was over 525 °C, the PCL was completely removed. On the other hand, in the DTA profile, an endothermic reaction occurred at around 60 °C, and two exothermic reactions occurred at around 360 and 420 °C due to decomposition of the PCL. In the case of the PMMA powder shown in Fig. 2b, the TG profile shows that the percentage of weight decreased as the temperature increased to 340 °C, and at over 425 °C, the PMMA powder was fully removed. The DTA profile shows that an endothermic reaction occurred at around 380 °C due to decomposition of the PMMA powder. However, in Fig. 2c, the steep weight loss, which occurs between 280 °C and 400 °C, can be ascribed to the decomposition of PMMA and PEG. In this stage, an endothermic reaction occurred at 310 °C in the DTA profile, respectively. Two exothermic reactions occurred at 384 °C and 412 °C due to the decomposition of little remnant of PMMA and PEG. The complete removal of PMMA and PEG also confirmed at over 425 °C.

Figure 3 shows SEM micrographs of porous BCP composites depending on the sintering temperature.

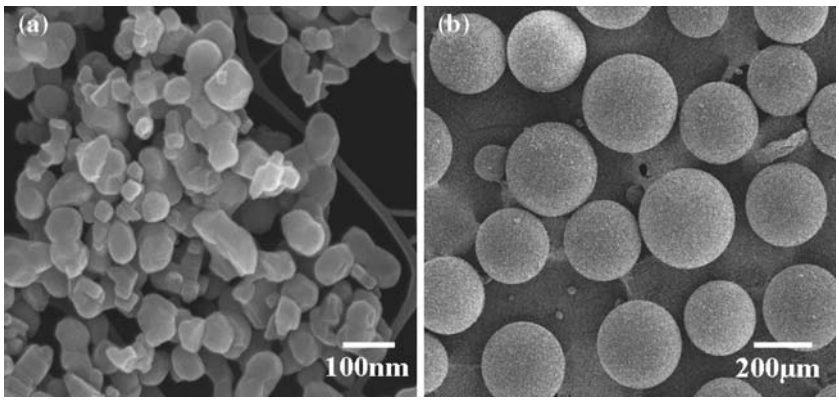

Fig. 1 SEM micrographs of (**a**) raw BCP and (**b**) PMMA powders

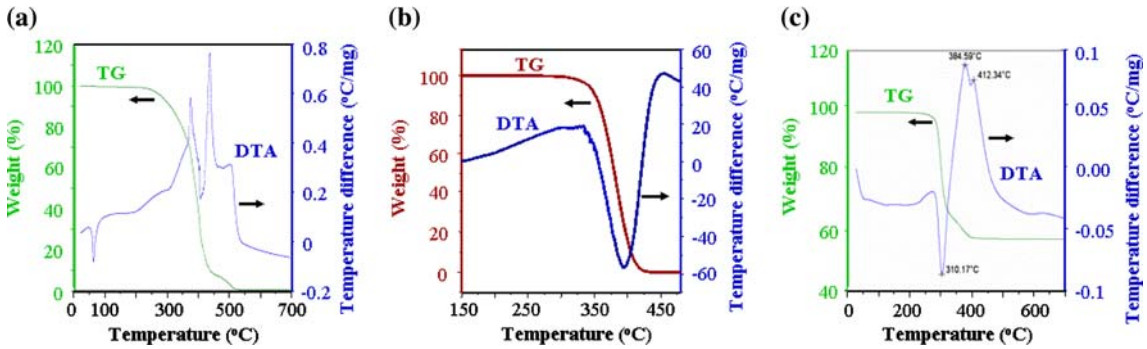

Fig. 2 TG/ DTA profiles of (**a**) PCL, (**b**) PMMA powders and (**c**) green pellet

Figure 3a and b were taken from the samples sintered at 1,200 and 1,400 °C, respectively and Fig. 3c shows an enlarged image of (b). After the 2nd burn-out and sintering processes, the PMMA, which was used as a pore-forming agent, was completely removed. The pores were spherical, about 200 μm in diameter, and showed an interconnected porous structure, which was clearly observed in Fig. 3c.

Figure 4 shows SEM micrographs and EDS profiles of the pore frame of porous BCP bodies depending on the sintering temperature. In Fig. 4a sintered at 1,200 °C, many fine grains about 0.5–2 μm in diameter were observed, but a few residual pores were also found. On the other hand, Fig. 4b shows remarkable grain growth of about 1–6 μm of β-TCP and densification of the pore frame were also improved. Thus, the residual pores were hardly observed. The EDS profiles (Fig. 4c, d), which were taken from Fig. 4b, showed that the atomic% of Ca and P in Fig. 4c were 14.45 and 9.57 (Ca/P = 1.51). However, the atomic ratio of Ca and P in Fig. 4d was 1.67 (atomic% of Ca and P were 20.06 and 12.01). These results revealed the existence of HAp phase in the porous BCP bodies sintered at 1,400 °C. The relative density of porous bodies also increased as the sintering temperature increased, as shown in Table 1.

Figure 5 shows XRD profiles of porous BCP bodies, which were (a) burned out at 700 °C, (b) sintered at 1,200 °C, and (c) 1,400 °C. These profiles revealed that major and minor phases were β-TCP and HAp, respectively, although the intensity of the HAp phase slightly decreased as the temperature increased. The existence of the HAp phase was confirmed in Fig.4a, b with fine particles as indicated with arrowheads and their EDS profiles in Fig. 4c, d.

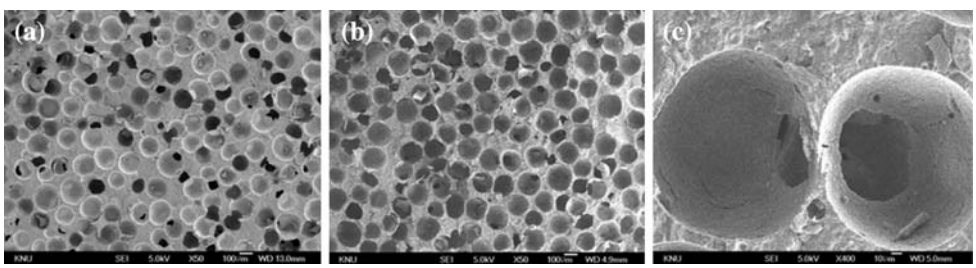

Fig. 3 SEM micrographs of porous BCP composites depending on sintering temperature (**a**) 1,200 °C, (**b**) 1,400 °C, (**c**) enlarged image of (**b**)

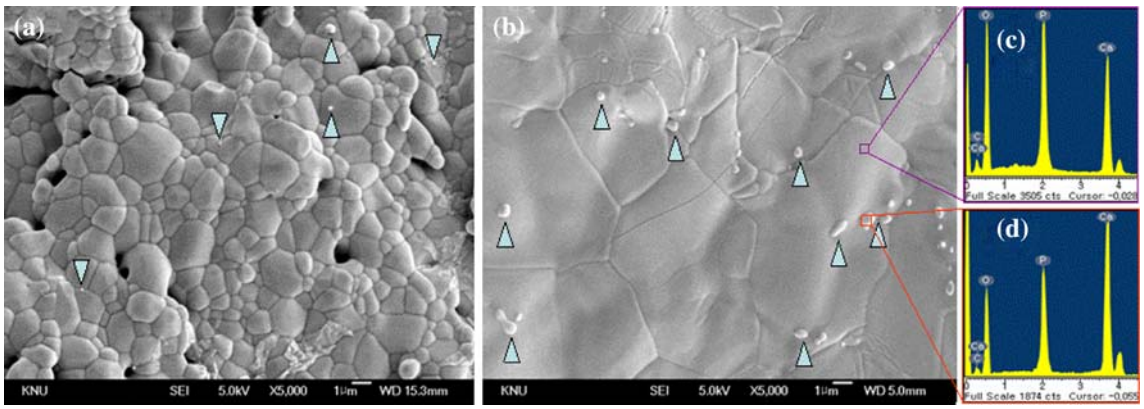

Fig. 4 SEM micrographs of porous BCP depending on the sintering temperature (**a**) high magnification of 1,200 °C, (**b**) high magnification of 1,400 °C and (**c**, **d**) EDS profiles

Table 1 Material properties of porous BCP and BCP/PCL composites

	Relative density (%)		Density (g/m^3)
	1,200 °C	1,400 °C	
Porous BCP	22.1	31.5	–
BCP/PCL	95.7	96.9	1.8
Human bone	–	–	1.6–2.1

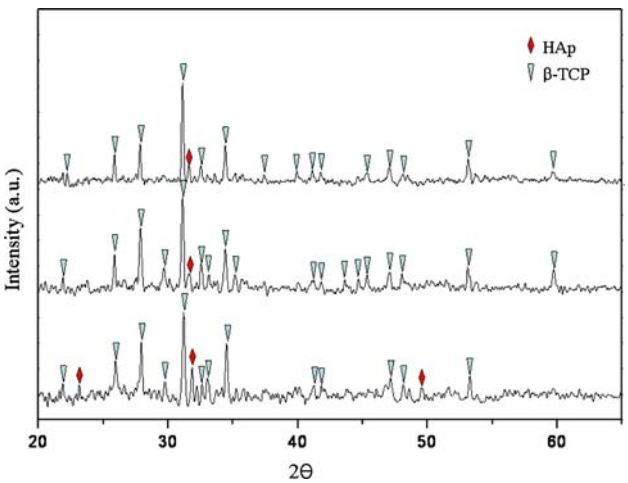

Fig. 5 XRD profiles of porous BCP bodies (**a**) burned-out at 700 °C, (**b**) sintered at 1,200 °C and (**c**) sintered at 1,400 °C

Figure 6 shows (a) a plane and (b) a cross sectional view of SEM micrographs of BCP/PCL composites using a porous BCP body which was sintered at 1,200 °C. In the plane view observation, the pore regions were fully infiltrated with PCL; thus, no residual pores were found. However, in a few local regions in the cross sectional observation, a few small gaps which were formed by incomplete infiltration of PCL into pores were observed at the BCP/PCL interface, as indicated with an arrowhead.

Figure 7 shows SEM micrographs of BCP/PCL composite, using a porous BCP body sintered at 1,200 °C. The low magnification image (a) shows an indentation site made by Vickers hardness as marked with a dotted line. Many microcracks were observed at the BCP frame which, shows significant crack deflection, as indicated by arrows. In the enlarged image (b) when the cracks propagated into the BCP frame, they showed straight propagation due to their intrinsic brittleness. However, in some regions, the cracks were propagated along the BCP/PCL interfaces.

Figure 8 shows SEM micrographs of fracture surface of BCP/PCL composites depending on the sintering temperature of porous BCP bodies. In Fig. 8a using porous BCP body which was sintered at 1,200 °C, the fracture surface was seen with rough, but the pulled-out spherical PCL was hardly observed. This observation means that the interfaces between BCP/PCL are comparatively strong bonding. However, in Fig. 8b (sintered at 1,400 °C), many pulled-out PCL spheres and their traces were observed on the fracture surface as well as microcracks. The main reason for showing the rougher surface is the low fracture toughness of BCP frame due to the grain growth of BCP frame. The material properties of BCP/PCL composites are shown in Table 2. The values in the sample sintered at 1,200 °C were higher than that of 1,400 °C due to the existence of fine grains. The value of elastic modulus was controlled in range of that of human bone and their values were about 9–10 GPa. However, the value of bending

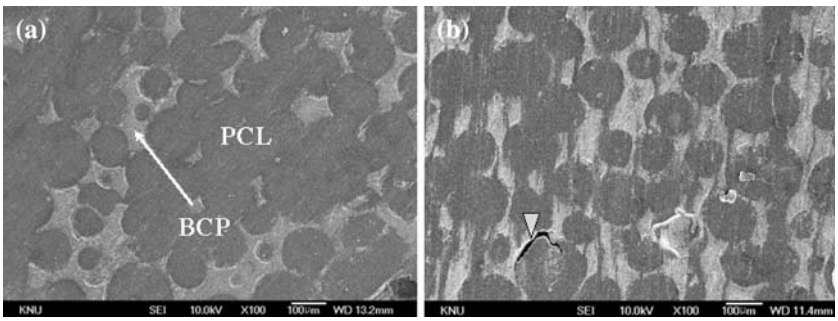

Fig. 6 SEM micrographs of BCP/PCL composites using porous BCP bodies which were sintered at 1,200 °C (**a**) plane view and (**b**) cross sectional view

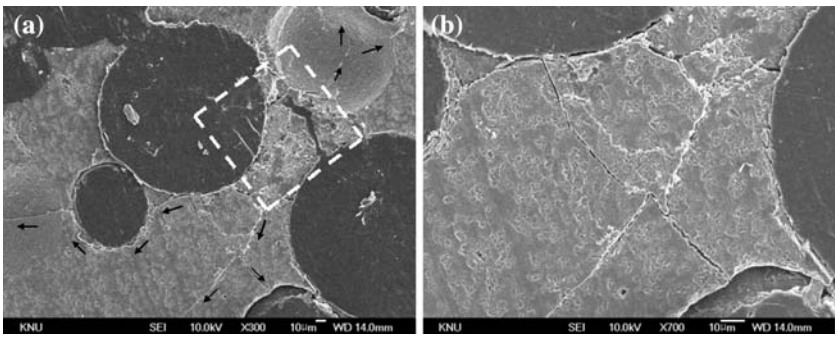

Fig. 7 SEM micrographs of BCP/PCL composites using porous BCP bodies which were sintered at 1,200 °C (**a**) low magnification and (**b**) high magnification of cracks

strength of BCP/PCL composites was 25–31 MPa which is slightly lower than that of human bone.

Figure 9 shows SEM micrographs of the fracture surface of BCP/PCL composites using porous BCP bodies which were sintered at 1,400 °C. In the low magnification image (a) traces of spherical PCL were frequently observed due to the pulled-out PCL phase. Thus, the main fracture of BCP/PCL composites showed an inter-granular fracture and some cracks were observed on the fracture surface as indicated with an arrow. However, the individual fracture modes of BCP and PCL were mixed with inter-granular and trans-granular types. Figure 9b shows a typical mixture fracture mode which frequently appears in brittle ceramics; the flat, rough regions correspond to typical trans-granular and inter-granular fracture modes. Figure 9c shows a typical trans-granular fracture of a spherical PCL phase which was infiltrated into the porous BCP body. The main fracture surface of the spherical PCL phase was observed with a cyclonic wave mode, having a rough surface due to the tearing of the molecular chain.

Figure 10 shows TG/DTA profiles of BCP/PCL composites. The TG profile is almost similar to TG profile which was shown in Fig. 2a, and it confirmed that the PCL was removed completely at over 500 °C. On the other hand, in the DTA profile, there are some exothermic reactions due to the decomposition of the PCL. However, these reactions were quite weak. Two other exothermic reactions occurred at around 432 °C and 462 °C due to the decomposition of little remnant of PCL.

In general, for application as a bone substitute, material properties such as fracture strength and elastic modulus as well as biocompatibility should be controlled and have values similar to those of human bone. If the fracture strength is lower than that of human bone, the artificial bone substrate can easily collapse during operation or during the implant application. Furthermore, if the elastic

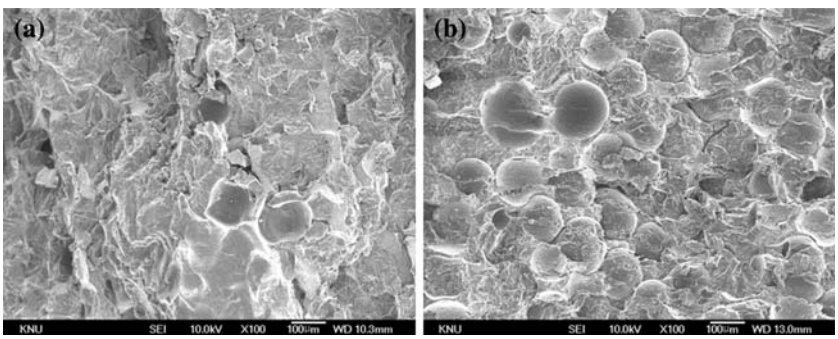

Fig. 8 SEM micrographs of fracture surface of BCP/PCL composites depending on the sintering temperatures of porous BCP bodies (**a**) 1,200 °C and (**b**) 1,400 °C

Table 2 Material properties of BCP/PCL composites

Sintering temperatures	Hardness (Hv)	Bending strength (MPa)	Elastic modulus (GPa)
1,200 °C	11.2 ± 0.5	31.6 ± 0.5	10.2 ± 0.5
1,400 °C	10.7 ± 0.5	25.7 ± 0.5	9.3 ± 0.5
Human bone	–	50–150	7–30

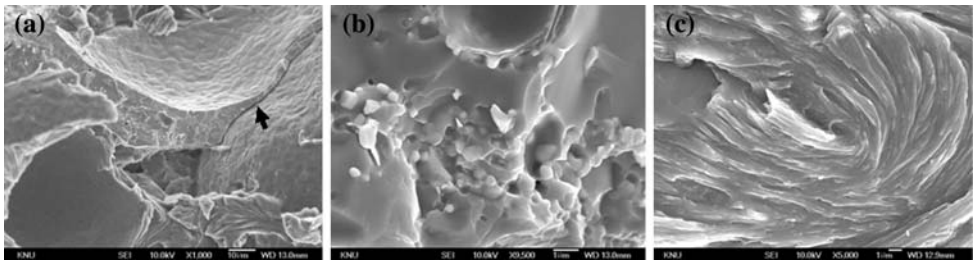

Fig. 9 SEM micrographs of fracture surface of BCP/PCL composites using porous BCP bodies which were sintered at 1,400 °C (**a**) low magnification, (**b**) high magnification of pore frame (BCP) and (**c**) high magnification of pore (PCL)

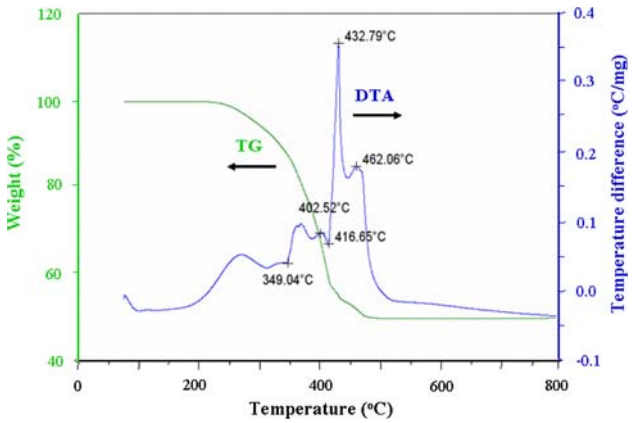

Fig. 10 TG/DTA profiles of BCP/PCL composites

modulus is remarkably higher than that of human bone, severe bone damage can occur due to stress shielding and stress concentration. In this work, the elastic modulus of BCP/PCL composites was controlled to obtain a value similar to that of human bone. However, the value of bending strength of BCP/PCL composites was slightly lower than that of human bone.

4 Conclusion

Porous BCP bodies were fabricated by pressure less sintering using 70 vol.% of PMMA powder as a pore-forming agent. The pore-forming agent was completely removed due to the burn-out and sintering processes. The porous bodies showed spherical, interconnected pores of about 200 μm in diameter and the densification of the pore frame was improved as the sintering temperature increased. BCP/PCL composites were fabricated by melt infiltration of PCL into porous BCP bodies, which were sintered at 1,200 and 1,400 °C. Most of the BCP pores were fully infiltrated by the molten PCL. The values of relative density, hardness, bending strength, and elastic modulus of BCP/PCL composites sintered at 1,200 °C were 95.7%, 11.2 Hv, 31.6 MPa and 10.2 GPa, respectively. As the sintering temperature of the porous BCP bodies increased, the intergranular fractures between the BCP and PCL phases increased. Thus, in the BCP/PCL composite sintered at 1,400 °C, many pulled-out PCL spheres and their traces were observed on the fracture surfaces as well as microcracks.

Acknowledgement This research was supported by a grant from the Center for Advanced Materials Processing (CAMP) of the 21st Century Frontier R&D Program funded by the Ministry of Commerce, Industry and Energy (MOCIE), Republic of Korea.

References

1. G. DACULSI, O. LABOUX, O. MALARD and P. WEISS, *J. Mater. Sci. Mater. Med.* **14** (2003) 195
2. R. Z. LEGEROS, S. LIN, R. ROHANIZADEH, D. MIJARES and J. P. LEGEROS, *J. Mater. Sci. Mater. Med.* **14** (2003) 201
3. H. S. RYU, H. J. YOUN, K. S. HONG, B. S. CHANG and C. K. LEE, *Biomaterials* **23** (2002) 909
4. K. DE GROOT, *Biomaterials* **1** (1980) 47
5. N. E. OZGUR and T. A. CUNEYT, *J. Euro. Ceram. Soc.* **19** (1999) 2569
6. L. YUBAO, C. P. A. T. KLEIN, Z. XINGDONG and K. DE GROOT, *Biomaterials* **15** (1994) 835
7. Y. LEI, B. RAI, K. H. HO and S. H. TEOH, *Mater. Sci. Eng. C* **27** (2007) 293
8. C. BIQIONG and S. KANG, *Polymer Test* **24** (2005) 978
9. K. REZWAN, Q. Z. CHEN, J. J. BLAKER and A. R. BOCCACCINI, *Biomaterials* **27** (2006) 3413
10. M. J. CURRAN, J. A. GALLAGHER and J. A. HUNT, *Biomaterials* **26** (2005) 5313
11. T. L. ARINZEH, T. TRAN, J. MCALARY and G. DACULSI, *Biomaterials* **26** (2005) 3631

12. X. WANG, H. FAN, Y. XIAO and X. ZHANG, *Mater. Lett.* **60** (2006) 455
13. H. R. R. RAMAY and M. ZHANG, *Biomaterials* **25** (2004) 5171
14. S. DEVILLE, E. SAIZ and A. P. TOMSIA, *Biomaterials* **27** (2006) 5480
15. M. H. YOUN, R. K. PAUL, H. Y. SONG and B. T. LEE, *Mater. Sci.* **534–536** (2007) 49
16. B. BALAKRISHNAN, D. S. KUMAR, Y. YOSHIDA and A. JAYAKRISHNAN, *Biomaterials* **26** (2005) 3495
17. J. SABBAGH, J. VREVEN and G. LELOUP, *Dent. Mater.* **18** (2002) 64